Assessing post-Miocene tilting of the Southern High Plains through paleoslope reconstructions of the Ogallala Formation

by

Audrey Pattat, B.S.

A Thesis

In

Geosciences

Submitted to the Graduate Faculty
of Texas Tech University in
Partial Fulfillment of
the Requirements for
the Degree of

MASTER OF SCIENCE

Dustin Sweet, PhD
Chair of Committee

Thomas Lehman, PhD

Harold Gurrola, PhD

Mark Sheridan
Dean of the Graduate School

August 2017

ACKNOWLEDGMENTS

First and foremost, I'd like to express my sincerest gratitude to my advisor, Dr. Dustin Sweet. He has been incredibly patient with me as I worked my way through this whole process. From providing the idea for this project, to helping with data collection and processing, and ultimately guiding me to the conclusions presented herein, he has made this a really enjoyable learning experience.

I would also like to thank my committee, Dr. Lehman and Dr. Gurrola, for helping me develop my understanding of this project and providing feedback and support throughout.

A huge thank you is owed to Rusty Winn, and the R.E. Janes Gravel Company, without whom this project would be standing on one leg (or rather, one data site). The R.E. Janes Gravel Co. allowed me to collect data from excavated sites on company property, which provided invaluable information. Rusty is the geologist for the company, and acted as a guide through the quarry, a narrator for depositional history at the site, and a field assistant while collecting data. His hospitality was second to none, and it was a joy to work with him in the field.

And finally, I don't think I would have made it through this process without the love and support of my family and friends, and my other half, Tanner.

TABLE OF CONTENTS

ABSTRACT

The Southern High Plains (SHP) is a physiographic region found in the panhandle of Texas and eastern New Mexico. The SHP is capped by an erosionally resistant caliche soil profile, the Caprock Caliche. Stratigraphy underlying the Caprock Caliche is largely fluvial and eolian deposition representing denudation of the Southern Rocky Mountains and Rio Grande Rift flank during the Miocene forming what is known as the Ogallala Formation. The dimensionless slope of the modern surface of the SHP and the base of the Ogallala Formation are both 0.0018. This slope is on the order of magnitude of proglacial alluvial fans, which do not hold a slope of this magnitude for more than 35 km from their source. Given the concave upward nature of fluvial downstream profiles, slopes should progressively shallow in distances past this 35 km. Deposits of the Ogallala Formation underlying the Caprock caliche are more than 300 km from their source land in the Southern Rocky Mountains. Considering this respective distance down fluvial profile, it seems unlikely that the modern slope is representative of the depositional slope of the Ogallala Formation. Paleoslope reconstructions were employed to estimate the slopes at which Ogallala Formation sediments were deposited at two sites using spatially averaged median grain size and paleoflow depth. Dimensionless depositional slopes were found to be 0.00018 and 0.00015—an order of magnitude less than the modern slopes of the surfaces bounding the Ogallala Formation. This implies the SHP has been tilted post-Miocene. Possible causes of tilting include: 1) recent tectonic activity, 2) isostatic uplift do to crustal heating, and 3) isostatic uplift due to erosion. No recent faulting has been reported in the study area capable of producing the amount of uplift necessary to

reconcile the difference in slopes. A 2-D isostatic model was built to test effects of lithospheric heating, possibly related to the Rio Grande rift, and isostatic rebound due to incision of the Pecos and Canadian rivers. Lowering lithospheric mantle density produced uplift on the order of nearly one kilometer. Removal of crust by the Pecos River induced 75 meters of uplift in the model, and incision of the Canadian River to the north of the SHP produced 82 meters of uplift. These values are likely overestimates as they do not account for lithospheric rigidity. Nearly 600 meters of differential uplift must have occurred near the western escarpment of the SHP to reconcile the difference in depositional and modern slopes for the Ogallala Formation. If crustal rigidity and concurrent uplift along the eastern margin of the SHP are factored in, the uplift modeled along the western margin the SHP from mantle heating and river incision accounts for the expected differential uplift along the western margin.

LIST OF TABLES

LIST OF FIGURES

CHAPTER I

INTRODUCTION

Rivers are one of the most powerful and pervasive agents that shape Earth's terrestrial realm. They are capable of stripping down mountain ranges and redistributing sediment hundreds to thousands of kilometers away. Removing significant quantities of material in turn affects isostatic equilibrium of the crust, inducing uplift to restore balance. It has been shown that river incision can produce epeirogenic crustal motion in otherwise tectonically quiescent continental interiors (e.g., Leonard, 2002; McMillan et al., 2002; Wisniewski and Pazzaglia, 2002; Heller, et al., 2003; Cather et al., 2012), aided to different degrees by mantle activity. To show uplift or rotation has occurred, pre-uplift conditions have to be established. Several of these studies used fluvial gravel deposits from the Ogallala Formation beneath the Great Plains to estimate paleoslope (Leonard, 2002; McMillan et al., 2002; Heller et al., 2003; Cather et al., 2012), which represents the slope of the surface at the time of deposition. Comparing the depositional slope to the modern basal Ogallala surface showed that the modern slope was unreasonably steep and did not represent the depositional slope (e.g. Cather et al., 2012, fig. 11 therein). Uplift is commonly attributed to mantle processes with or without aid from river incision.

Similar observations concerning unreasonable steepness of modern Ogallala surfaces have been made on the Southern High Plains (SHP). Dimensionless slope along the surface of the SHP varies from 0.0010-0.0021, depending on the orientation of the slope profile. Modern drainage flows roughly W-E, and a profile along this

trend has a slope of 0.0020 (Fig. 1.1) This slope should mimic the depositional slope of the Ogallala Formation, as only a thin mantle of Quaternary eolian material covers the Ogallala deposits. Similarly, the basal Ogallala Formation surface has a dimensionless slope from W-E of 0.0018, measured from data presented by Seni (1980). These deposits are more than 300 km from their paleo-uplands along the eastern flanks of the Rio Grande Rift to the west in New Mexico, and given the concave upward nature of slope profiles for rivers, these modern slope values appear steepened. To evaluate this possibility, a database of modern North and South American river slopes was assembled and plotted versus distance from the highland

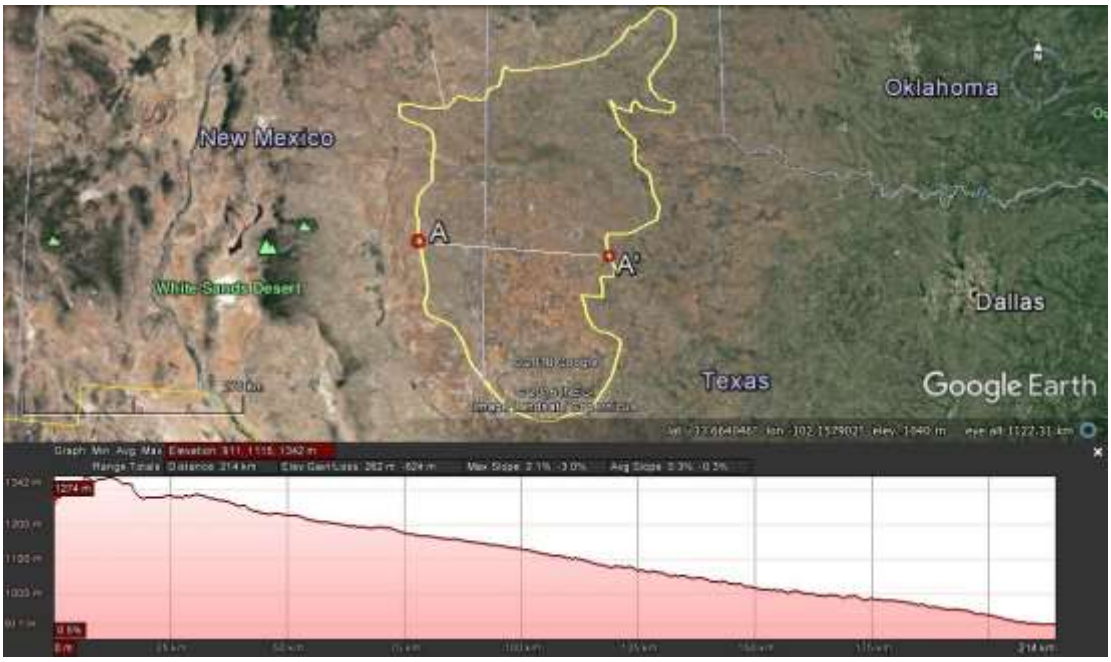

Figure 1.1. Topographic profile of the modern SHP surface. SHP is outlined in yellow. The profile runs W-E, in accordance with modern drainage patterns. Dimensionless slope of this surface = 0.0020. Vertical exaggeration of profile = ~500X. Map data ©2016 Google.

away from which the rivers are flowing (Fig. 1.2; Appendix A). Modern Ogallala Formation slopes were taken between 300-400 kilometers from the highlands in eastern New Mexico. Comparing the observed Ogallala slope to this database supports the hypothesis that the observed slope is steepened through post-depositional uplift. This study seeks to further investigate if the SHP has been tilted post-Miocene through reconstructing depositional slope of the Ogallala Formation, comparing depositional slope to the modern slope, and providing a potential explanation for the cause of any observed tilting.

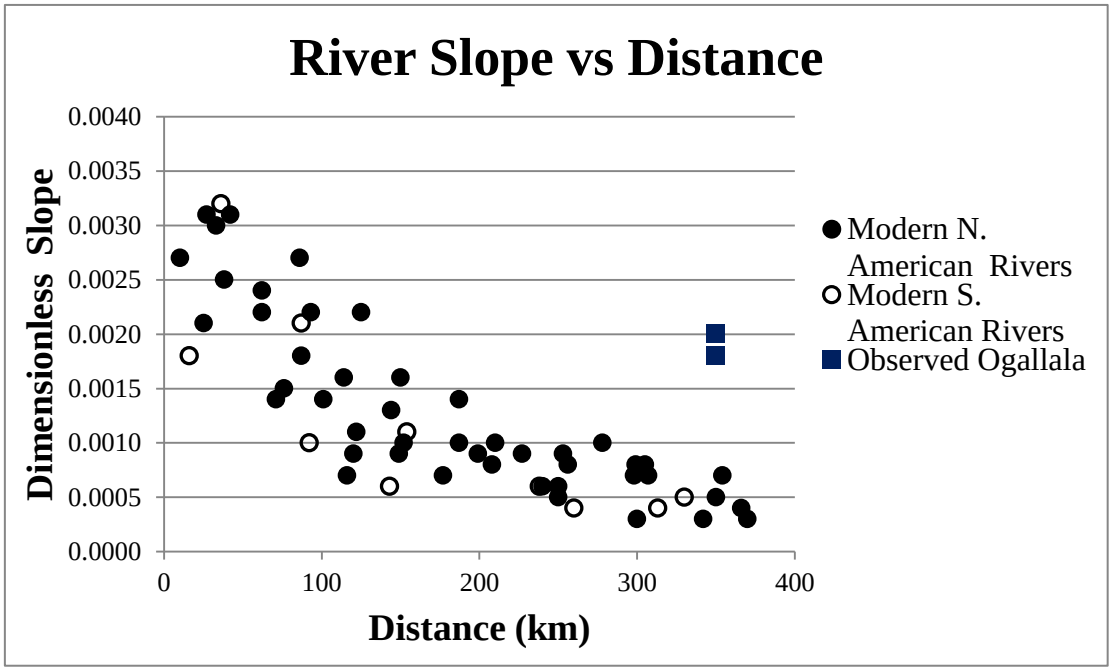

Figure 1.2. Plot of dimensionless slope versus distance for modern rivers. North American river data points were measured along the eastern flank of the Rocky Mountain Cordillera. South American data points were taken from the eastern flank of the Andes Mountains. Observed Ogallala slopes represents both the slope of the SHP surface, and the basal surface slope of the Ogallala Formation. Plot data is presented in Appendix A.

CHAPTER II

GEOLOGIC SETTING

The Southern High Plains

The Southern High Plains (SHP), also known as the Llano Estacado, is a subaerial plateau covering ~80,000 km^2 in southeastern New Mexico and the panhandle of north Texas (Fig. 2.1). The SHP is the southernmost section of the North American Great Plains, and sits 1400-900 m above sea level. A significant portion of the plateau-building sediments are recent, and are partially-to-completely unconsolidated (Bretz and Horberg, 1949). A period of arid conditions in early Pliocene is responsible for the development of the Caprock Caliche, a thick, erosionally resistant layer that acts as a "lid" atop the plateau, slowing the removal of sediment and prolonging the life of this topographic high (Bretz and Horberg, 1949; Walker, 1978). River incision spanning from the Pleistocene through the present has cut through the Caprock Caliche and carved the escarpments that form the edges of the modern plateau (Bretz and Horberg, 1949; Walker, 1978). The SHP was isolated from the northern High Plains by headward erosion of the Canadian River (Walker, 1978). Western and southern margins of the plateau are the result of incision and lateral migration of the Pecos River, while headcutting of the Red, Colorado, and Brazos rivers have carved the eastern escarpment (Walker, 1978). The southeastern-most portion of the SHP transitions less markedly into the Edwards Plateau (Reeves, 1976). The modern SHP exhibits a relatively planar surface that gently dips to the east (Walker, 1978).

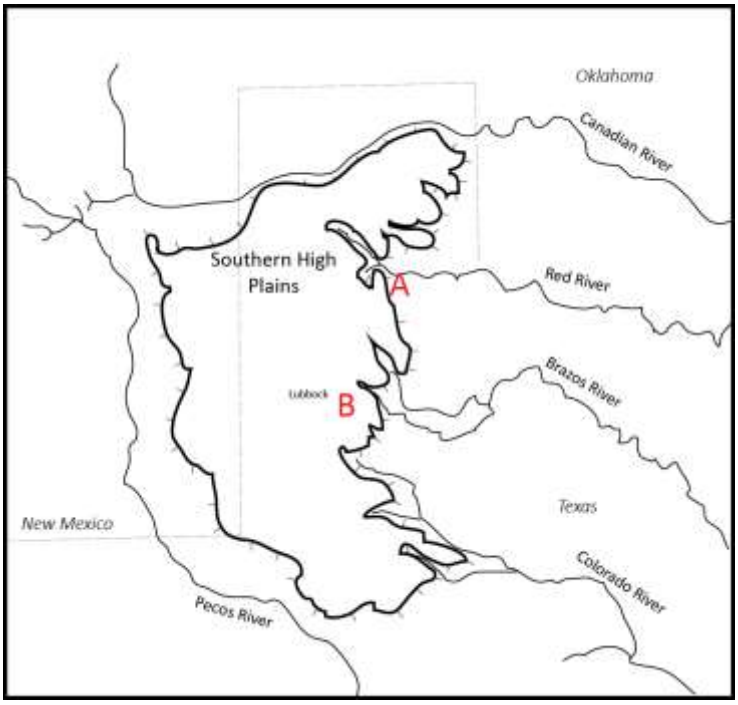

Figure 2.1. Regional map showing the outline of the Southern High Plains. The area is bounded: 1) to the north by the Canadian River valley; 2) to the west by the Mescalero Escarpment and the Pecos River valley; 3) to the east by the Caprock Escarpment. Field sites A and B shown. (After Walker 1978)

Stratigraphy of the SHP

Stratigraphy exposed along the modern escarpments of the SHP ranges from Permian through Quaternary in age. Differences in stratigraphic nomenclature are used based on location, mainly eastern New Mexico versus Texas (Fig. 2.2). Incision of the Pecos River to the west of the SHP has exposed the strata that comprise the western plateau in New Mexico (Reeves, 1976; Walker, 1978). Near Santa Rosa, NM, this incision has exposed the upper Permian Artesia Group which is predominately dolomite and sand strata (Cox, 1967). Above lie Triassic strata collectively called the Dockum Group (Barnes et al., 1977). Jurassic strata appear above the Dockum Group,

and include the Exeter Sandstone overlain by shale, claystone, and sandstone strata comprising the Morrison Formation (Barnes et al., 1977). Cretaceous strata include the Tucumcari Shale, Mesa Rica Sandstone, and the Pajarito Shale (Barnes et al., 1977). An unconformity sits atop the Cretaceous interval and separates it from Cenozoic strata above (Walker, 1978; Seni, 1980). Approximately 38 m of Cenozoic strata are exposed in the Pecos River valley, including 30 m of fluvial sand and gravel known as the Ogallala Formation, and 8 m of Quaternary eolian and alluvial deposits including the Tahoka and Blackwater Draw formations (Barnes et al., 1977).

River incision along the eastern escarpment of the SHP has exposed strata sitting beneath the surface of the Texas portion of the plateau. The oldest exhumed units are the Permian White Horse Group and overlying Quartermaster Formation, made of predominately siltstone and gypsum (Lucas and Anderson, 1993). Overlying Permian strata are a series of Triassic-age shale, siltstone, and sandstone beds collectively known as the Dockum Group (Eifler et al., 1967). Jurassic-aged strata are not seen along the eastern escarpment. Locally, Cretaceous strata sit unconformably over the Dockum Group, and are made of the Antlers Sandstone, Walnut Formation, and Comanche Peak Limestone (Eifler et al., 1967). Another unconformity separates Cretaceous strata from the overlying Cenozoic deposits (Walker, 1978; Seni, 1980). At the base of the Cenozoic succession is the Ogallala Formation, which constitutes a majority of the Cenozoic thickness at 46-76 m of fluvial and eolian sand and local gravel (Bretz and Horberg, 1949; Eifler et al., 1967; Walker, 1978; Gustavson and Winkler, 1988). Above the Ogallala Formation lies the Quaternary Blackwater Draw Formation, a sheet-like deposit of eolian sediments measuring 9 m thick at the type

section (Holliday, 1990). Locally, lacustrine deposits are inset into the Ogallala Formation, including the Tule and Blanco formations, but they do not add to the overall thickness of the Cenozoic succession (Fig. 2.3) (Reeves, 1976; Holliday, 1990).

New Mexico		**Texas**
Tahoka Formation Blackwater Draw Formation Ogallala Formation	Cenozoic	Tahoka, Tule and Blanco Formations Blackwater Draw Formation Ogallala Formation
Pajarito Shale Mesa Rica Sandstone Tucumcari Shale	Cretaceous	Comanche Peak Limestone Walnut Formation Antlers Formation
Morrison Formation Exeter Sandstone	Jurassic	Unobserved
Dockum Group	Triassic	Dockum Group
Artesia Group	Permian	Quartermaster Formation White Horse Group

Figure 2.2. SHP stratigraphic column. Stratigraphic column showing differences in nomenclature for SHP strata in New Mexico versus Texas.

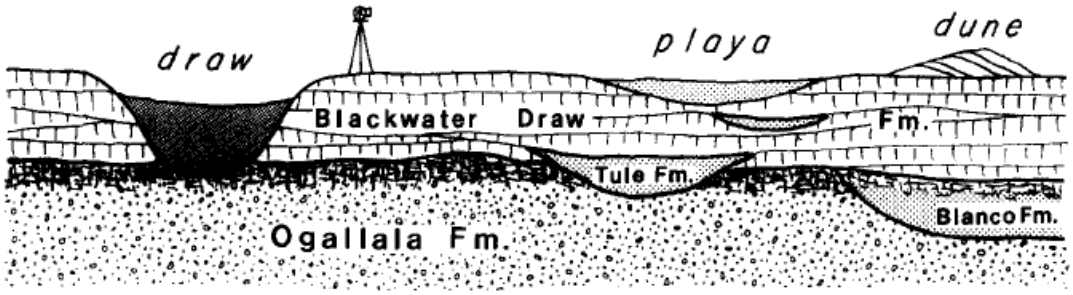

Figure 2.3. Sketch of Cenozoic deposition on the SHP (From Holliday, 1990).

The Ogallala Formation

Flat-slabbed subduction during the latest Cretaceous to Paleogene produced thick-skin deformation within the midcontinent known as the Laramide Orogeny, resulting in basement-cored uplifts in the Rocky Mountain region (Dickinson and Snyder, 1978) and generally positive topography across the midcontinent. Uplifts associated with this orogeny (Fig. 2.4) provide the source terrain and buttress for the Ogallala piedmont through the Great Plains, while volcanism along the eastern flank of the Rio Grande Rift zone acted as a source for Ogallala sediments in the south (Bretz and Horberg, 1949; Walker, 1978; Hawley, 1993). The Ogallala Formation records a widespread blanket of sediment that spread out along the eastern margin of theses highlands during the Miocene (Walker, 1978). It is laterally extensive, spanning from the southern border of South Dakota through the panhandle of northern Texas (Walker, 1978) (Fig. 2.5). Sediments were transported great distances from their source (200-350+ km) by eastward-flowing rivers (Walker, 1978; Heller et al., 2003), with lesser contribution from eolian processes (Walker, 1978; Gustavson and Winkler,

1988; Winkler, 1990). The Ogallala Formation is economically significant as a primary aquifer for the farming regions of the Great Plains.

Figure 2.4. Paleogeographic reconstruction of North America at 60 Ma. The Western Interior Seaway has fully retreated due to Laramide uplift. Southern High Plains outlined in red. (From Blakey, 2011).

Ogallala Formation of the Southern High Plains

The Ogallala Formation makes up most of the Cenozoic sediments forming the SHP, with the only continuous overlying unit being a thin, wind-blown mantle of Blackwater Draw Formation (Bretz and Horberg, 1949; Reeves, 1976; Walker, 1978, Seni, 1980). The Ogallala Formation was deposited upon on erosional surface of late Cretaceous through early Miocene age (Fig. 2.6; Walker, 1978). In the north, the Ogallala Formation was deposited upon a series of solution collapse features

developed in Permian evaporites (Cronin, 1969; Seni, 1980), within which the thickest sequences of Ogallala sediment are found, up to 250 meters thick (Seni, 1980). South

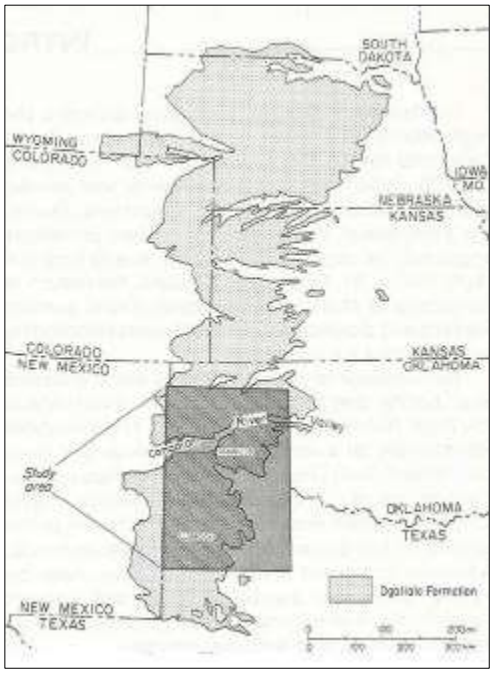

Figure 2.5. Map showing the extent of the Ogallala Formation (light gray). From Seni (1980).

of this area, Triassic or younger strata were not removed, inhibiting development of these collapse features (Seni, 1980). Instead, to the south, paleo-channels incised into Triassic and Cretaceous strata and formed a series of northwest to southeast trending paleovalleys (Walker, 1978; Seni, 1980; Gustavson and Winkler, 1988). These valleys have been interpreted by some to be the first areas to fill with Ogallala sediments (Seni, 1980; Gustavson and Winkler, 1988).

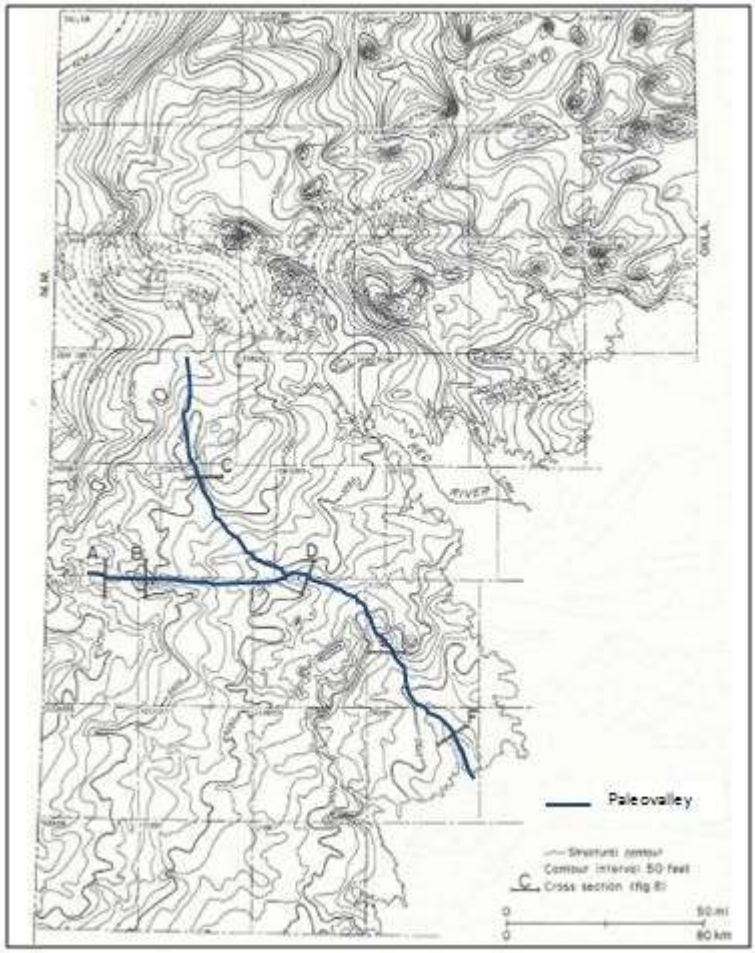

Figure 2.6. Contour map of the base of the Ogallala Formation. The depositional surface slopes to the southeast. The northern portion shows a series of closed depressions. These were formed by solution collapse of Permian-aged evaporite deposits. Outlined in blue is the approximate location of an ancient river system that carved out valleys. After Seni (1980).

Depositional environment of the Ogallala Formation is debated. Some interpretations invoke modern humid alluvial fans (Johnson, 1901; Bretz and Horberg, 1949; Seni, 1980); whereas, more infer cycling between fluvial and eolian systems

driven by changing climate (Winkler, 1987, 1990; Gustavson and Winkler, 1988). The latter is most widely accepted today, and it is the model this study will follow.

Correlation is difficult in the Ogallala Formation due to the absence of internal regional surfaces (Gustavson and Winkler, 1988; Winkler, 1990). Therefore, the unit has been subdivided based on sedimentological changes into the Couch and Bridwell members (Fig. 2.7; Evans, 1949; Walker, 1978; Gustavson and Winkler, 1988; Winkler, 1990). This relationship has only been extensively studied and mapped in Blanco and Yellow House canyons along the eastern escarpment (Gustavson and Winkler, 1988; Winkler, 1990), but the nomenclature is generally used when describing the Ogallala Formation on the SHP. The lower half of the Couch Member is dominated by sand and gravel inferred as fluvial channel-fill facies (Winkler 1990). Gravel often lines the base of these channels (Winkler, 1990). Locally, crossbedding occurs in channel fill and ranges from 0.1 to 1 m high (Winkler, 1990). Above the channel facies lies an erosional surface, overlain by a massive silty sand facies with local pedogenic carbonate, which comprises the upper portion of the Couch Member (Winkler, 1990). The basal surface of the Bridwell Member is erosive, and scours into the upper Couch Member (Winkler, 1990). Channel facies compose more than half of the Bridwell Member in the composite section presented by Winkler (1990), interrupted at two depths by the massive silty sand facies (Fig. 2.7; Winkler, 1990). At this locality, the upper third of the Bridwell Member is comprised of laminated mudstone beds with minor silt and fine sand that commonly contain root traces and burrows (Winkler, 1990). At the top of the Bridwell Member sits the Caprock Caliche

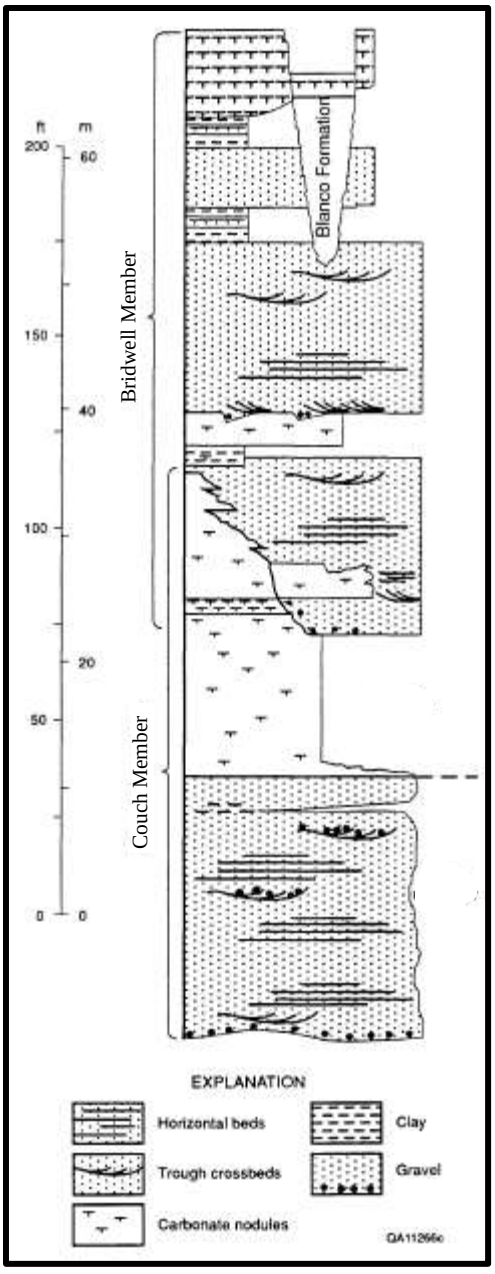

Figure 2.7. Stratigraphic column of the Ogallala Formation on the SHP. The formation is made up of two members—the Couch and Bridwell. Each member represents a climate cycle: early deposition occurred during sub-humid climate and is dominated by fluvial deposits. The climate shifts from sub-humid to sub-arid, invoking a change from fluvial to eolian deposition. From Winkler (1990).

described by Holliday (1990) as having Stage V-VI structure, which suggests a pedogenic duration of approximately 0.5 to 2 million years in warm, semi-arid climate (Machette, 1985).

Interpretation of facies is closely tied to changes in climate during Ogallala deposition. Channel facies lack significant mud, which is the basis for an inferred ephemeral sandy braided stream setting (Walker, 1978; Winkler, 1990). Lack of mud implies that the channel banks would be non-cohesive. The ephemeral nature of the streams would imply that the climate was capable of producing periods of precipitation, but not humid enough to supply enough runoff to make streams perennial. The overlying silty sand facies are interpreted to represent a change from a fluvial system to an eolian system due to a drying of the climate (Reeves, 1976; Walker, 1978; Gustavson and Winkler, 1988; Winkler, 1990). Presence of pedogenic carbonate in this facies helps corroborate increasing aridity during this phase of deposition. Lack of major sedimentary structures in the eolian units may be due to lack of available sediment, forming sand sheets rather than dunes (Winkler, 1990). Reintroduction of fluvial facies at the base of the Bridwell Member indicates the climate shifted back to more humid conditions. Brief periods of dryness are evidenced by the relatively thin episodes of the silty sand facies followed by recurrence of fluvial facies (Winkler, 1990). A final shift to aridity ended fluvial deposition near the top of the Bridwell Member, and an extended period of dry conditions led to soil formation and vegetation in the mud layers seen there (Walker, 1978; Gustavson and Winkler, 1988; Winkler, 1990). These arid conditions culminated in the Caprock Caliche, and extended through much of the Pliocene (Walker, 1978, Holliday, 1990). This caliche

surface remained at the top of the SHP until the Blackwater Draw Formation began to form and cover the SHP during Illinoian glaciation in the Pleistocene (Reeves, 1976; Holliday, 1989).

Absolute age dating of the Ogallala Formation is difficult due to lack of crystalline rock and scarcity of through-going volcanic ash beds. Researchers have resorted to the best available method for constraining the timing of Ogallala deposition—mammal fossils. North American mammal fossils of the Cenozoic have been studied and arranged in biochronological order, establishing what was originally known as Provincial Mammal Ages, and has evolved into the North American Land Mammal Ages. These ages are used to tell time independent of the lithology and the geologic time scale in Cenozoic terrestrial strata, although they are often correlated to the time scale (Woodburne, 2004). Mammal fossils found in the Ogallala Formation include abundant and varying types of horses, as well as camels, oreodonts, rhinoceroses, ground sloths, canids, and saber tooth cats, among others (Cope, 1893; Schultz, 1977, 1990; Tedford, et al., 2004; Winkler 1987, 1990). Ogallala Formation mammals fall into the middle Clarendonian (Couch Member) through Hemphillian (Bridwell Member) land mammal ages (12 Ma-4.8 Ma) (Tedford, et al., 2004; Schultz, 1990), and, in fact, type localities for these ages occur in Ogallala strata on the Great Plains and SHP (Tedford, et al., 1987; Tedford, et al., 2004). A volcanic ash near the middle of the Bridwell Member has been dated 6.8 ± 0.2 Ma (Izett and Obradovich, 2001), supporting the age proposed by the mammal fossils.

CHAPTER III

METHODS

Paleoslope Calculation

To test the hypothesis that the SHP has been tilted post-Miocene, a depositional slope for Ogallala sediments was estimated using an established method of paleoslope reconstruction (Paola and Mohrig, 1996) and compared to both the slope of the modern surface of the SHP and the basal surface of the Ogallala Formation. Paola and Mohrig (1996) developed a theoretical relationship of grain size and water depth to depositional slope for gravel-dominated bed load streams, which was shown to agree within a factor of two when tested against modern rivers. The relationship is applicable to ancient rivers that would have self-adjusted to increases in discharge through variations in channel width, not depth (i.e. rivers with non-cohesive banks), to maintain a temporally and spatially averaged critical bed shear stress. This method is based on principles of a force balance represented by:

$$\tau_0 = \rho g h S \quad (1)$$

where τ_0 represents boundary shear stress, ρ represents fluid density, g represents acceleration due to gravity, h represents fluid flow depth, and S represents slope. The force balance is between shear stress created during fluid flow (boundary shear stress), left side of the equation, and the resistance to that flow, right side of the equation. If resisting forces are greater than the shear stress, a particle resting on the bed will not move. Once shear stress surpasses resisting forces, particle motion is initiated. τ_{0c} is defined as the critical shear stress required to initiate motion of a particle. Critical

shear stress is controlled by the depth and slope of the system, and the latter also controls stream velocity. Paola and Mohrig (1996) made the case that in rivers without cohesive banks, a river will accommodate increased discharge predominantly by widening its banks, rather than incising into the substrate, meaning the depth of flow will not vary greatly. Therefore, if depth of a channel is considered relatively constant, then critical shear stress is primarily a function of the slope of the system. To increase critical shear stress and transport larger grain sizes across the length of the fluvial system, the system's slope must be increased. Parker et al. (1982) found that for a sample of mixed grain sizes (as would be expected in fluvial sediment), that a state of 'equal mobility' can occur where motion is initiated on all grain sizes in a sample of sediment at the same critical shear stress, and this shear stress is a function of the median grain size of the sample (D_{50}). Paola and Mohrig (1996) incorporated this into their model, yielding the theoretical relationship of grain size and water depth to the slope of a river. This estimation quantifies depositional slope in bedload river deposits lacking cohesive banks with a minimum median grain size of 2 mm (i.e. gravel). The grain-size restriction is based on the reasoning that gravel-sized material will be transported primarily by bedload processes, rather than suspension, as required by the critical shear stress relationship. The resulting paleoslope relationship is shown in Equation 2:

$$S_{est} = \frac{.094 \cdot <D_{50}>}{<h>} \quad (2)$$

Here, $<D_{50}>$ represents spatially averaged median grain size of bedload material sampled vertically and laterally through a deposit, and $<h>$ represents spatially averaged flow depth.

Site Characterization

Two field sites were used for Ogallala Formation data collection on the SHP, and their locations are marked on Figure 2.1. Presence of abundant gravel, cross stratification, and lower plane bed structures indicated that the sites were in the fluvial facies of the Ogallala Formation. Field Site A is located in Caprock Canyons State Park, on the eastern escarpment of the SHP near the Prairie Dog Town Fork of the Red River. Samples and measurements taken at this site (Fig. 3.1) represent fluvial deposits in the Couch Member of the Ogallala Formation. Cross-bedding thicknesses and samples for grain-size analysis were collected from three locations at Field Site A (Fig. 3.2). Field Site B is located near Slaton, TX, in the R.E. Janes Gravel Co. quarry. Sediments at Field Site B have been interpreted as deposits in one of the paleovalleys cut prior to Ogallala Formation deposition known as the Slaton Channel (Seni, 1980; Gustavson and Winkler, 1988; Winkler, 1990). These deposits actually belong to the Bridwell Member of the Ogallala Formation, where rivers incised and removed any existing Couch Member deposits (Gustavson and Winkler, 1988). Again, three locations 2.5-5 kilometers apart were sampled at Field Site B for grain-size analysis and bedform thicknesses (Figs. 3.3-3.6).

Application of the paleoslope method operates on the assumptions that the deposits studied represent a river system lacking cohesive banks and dominated by bedload transport of sediment greater than two millimeters in diameter. Little to no mud was observed at either site, and presence of dune cross stratification implies deposition occurred via grain-by-grain bedload transport. Initial inspection of sediment in outcrop revealed abundant gravel, with most outcrops being gravel clast supported. Therefore, the Ogallala Formation outcrops studied meet the criteria and are suitable for this method.

Figure 3.1. Panorama showing Field Site A, located in Caprock Canyons State Park. Red line denotes the base of the fluvial strata sampled.

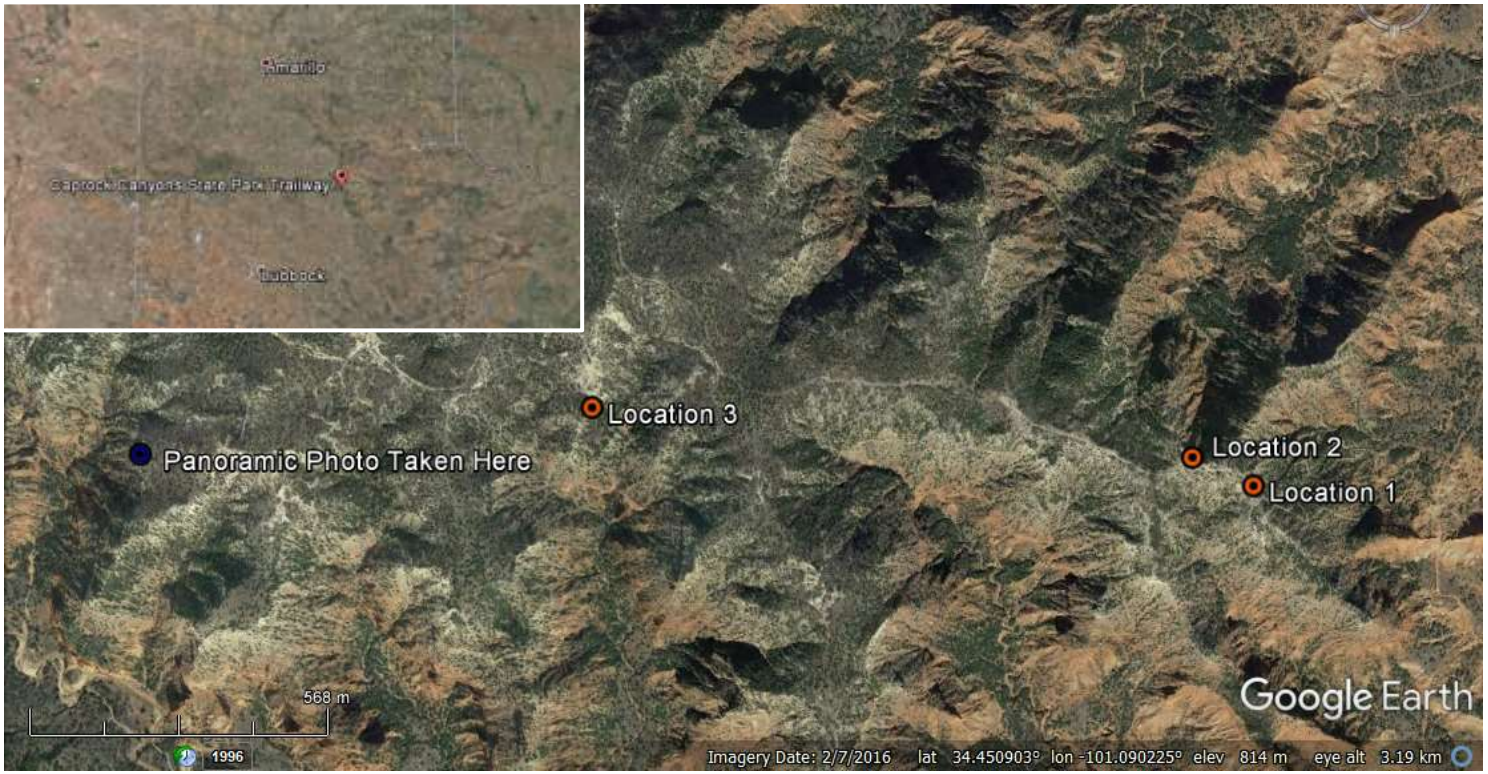

Figure 3.2. Field Site A sampling locations. Located in Caprock Canyons State Park. Location 1 and Location 2 are less than a kilometer from each other, separated by a ridge. Location 3 is ~1 kilometer from the other locations. Map data ©2016 Google.

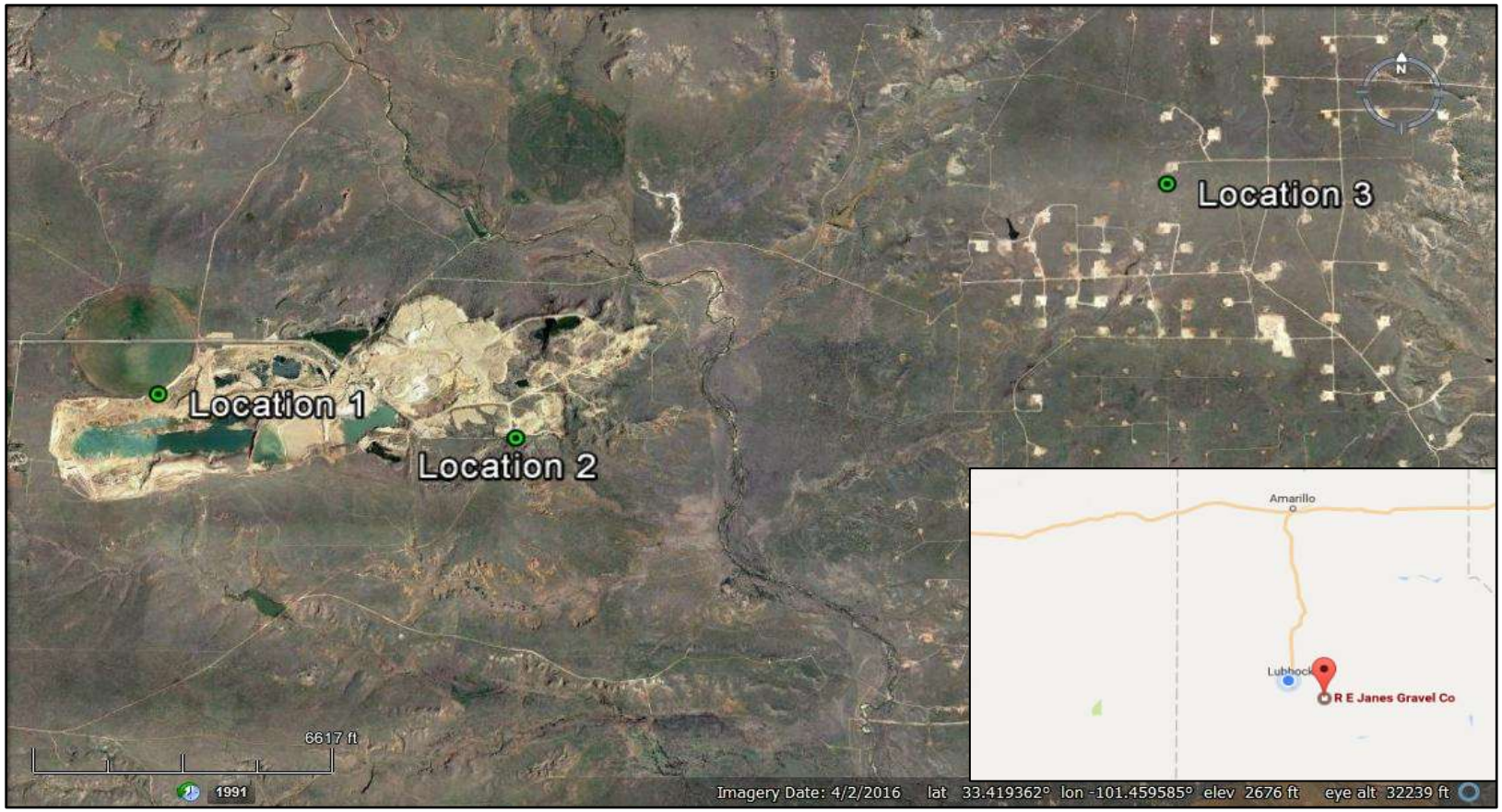

Figure 3.3. Field Site B sampling locations. Located near Slaton, TX, in the R.E. Janes Gravel Co. quarry. Location 1 is 2.5 kilometers from Location 2. Location 2 is 5 kilometers from Location 3. Map data ©2016 Google.

Figure 3.4. Panorama of Field Site B, Location 1.

Figure 3.5. Panorama of Field Site B, Location 2.

Figure 3.6. Panorama of Field Site B, Location 3.

Data

To perform calculations for the paleoslope reconstructions, spatially averaged median grain size $<D_{50}>$ and spatially averaged paleoflow depth $<h>$ had to be established.

Grain-Size Analysis

Grain-size analysis involved two processes: 1) point counting the coarse fraction (>1 cm) on images of outcrop; and 2) traditional sieving for the < 1cm fraction. Outcrop analysis utilized high-resolution images at the sampling locations, with a centimeter scale included in the pictures. A two centimeter grid was overlain on the images (Fig. 3.7), and at grid intersections, grain diameters were measured, similar to point counting in a thin section. Any intersection falling on grains less than one centimeter in diameter was counted as matrix. Approximately 300 counts were recorded per sampling location, totaling at least 900 counts each for sites A and B. For each sampling location, percentages were calculated for each one-centimeter bin, yielding the grain-size distribution for the > 1 cm fraction of the sediment.

The matrix fraction (< 1 cm) was too fine to be analyzed with digital images, so bulk sediment samples were collected from each sampling location for sieving. Matrix samples collected from the three sampling locations at sites A and B, and each sampling location was combined to form a single, representative matrix sample for the respective site. Samples were treated with acid to dissolve calcite and eliminate lithification (see Sample Preparation section below for details). Once samples had

Figure 3.7. Example of digital grain size analysis. Taken from Field Site B, Location 3. A 2-cm grid was overlain on outcrop images, and grain diameters were measured at grid intersections. An intersection falling on a grain less than 1 cm in diameter was counted as matrix.

been disaggregated, they were sieved. Sediment trapped in each sieve was weighed, and then weights were summed to get total matrix sample weight. Individual sieve weights were divided by the total sample weight to calculate weight percent for each sieve (see Appendix B for sieve set up).

The coarse and matrix fractions were normalized into a composite grain-size distribution for each sampling location yielding six grain-size distributions (Appendix B), three for Field Site A and three for Field Site B. For example, Field Site B, sampling location 1, contained 40% matrix. The sieve weight percent values for Field Site B were each multiplied by 0.40, since matrix only represented 40% of the overall sediment at location 1. D_{50} values were taken from each distribution and averaged for

the respective sites, resulting in a spatially averaged median grain size (<D_{50}>) for each field site.

Sample Preparation

Sediment samples were soaked in a diluted 10% formic acid solution until reaction slowed or completely stopped (24-48 hours). The acid solution was carefully drained off, then replaced by deionized water to rinse the sediment. Samples were left to settle (~24 hours) then the water was poured off. Samples were then placed in a drying oven to drive off remaining moisture before sieving.

Estimating Paleoflow Depth

Flow depth in a river is one of the main factors controlling shear stress and grain movement. Estimating flow depths from deposits is challenging, but various bedforms have been shown to scale to depth of flow. Allen (1968) presented a method for estimating flow depth for a given height of a dune, based on the empirical relationship between bedform height and flow depth in modern systems and laboratory experiments, shown in Equation 3, where *b* represents bedform height and *h* represents flow depth.

$$b = 0.086h^{1.19} \quad (3)$$

Therefore, to estimate flow depth in ancient fluvial systems, measurements of dune heights can be related back to their depositional flow depth (Eq. 4).

$$h = \sqrt[1.19]{\frac{b}{0.086}} \quad (4)$$

Ideally, a perfectly preserved dune would show the stoss side as well as the lee foresets. However, dunes are typically eroded as a new dune migrates over top of them, leaving only part of the foresets preserved as cross bedding. Thus, calculated flow depths are most commonly an underestimate. Alternatively to dune cross bedding, gravelly lower-stage plane bed that are overlain by finer gravel or sand are considered "incipient dunes" with the basal coarse gravel representing the armored bed between bedforms (Bridge and Demicco, 2008). The heights of these features have been shown to correlate with flow depths (Bridge and Demicco, 2008). Both structures were used in this study.

Dune and lower-stage plane bed heights were measured at each of the six sampling location, totaling 21 measurements for Field Site A and 23 measurements for Field Site B. All but three measurements for Field Site B were measured digitally using high-resolution outcrop photos (e.g. Fig. 3.8); measurements for Field Site A were taken on outcrop. For each sampling location, heights were averaged, then related back to flow depth using Equation 4. Then flow depths were averaged site-wise, resulting in a spatially averaged paleoflow depth (<*h*>) for each site.

Figure 3.8. Digital bedform measurement. Image of Field Site B, Location 2, showing digital measurements for bedform heights. Scale bar = 3 m.

CHAPTER IV

PALEOSLOPE CALCULATIONS

Grain-size distributions are shown in Appendix B. Median grain size (D_{50}) values for each sampling location are shown in Table 1. Spatially averaged median grain size ($<D_{50}>$) for sites A and B were 6.2 and 7.8 millimeters, respectively, fulfilling the paleoslope calculation requirement that median grain size is greater than two millimeters. These values were measured directly from samples so they should have inherently low error associated with them.

Table 4.1. Grain Size Data

Location	Median Grain Size (D50) (mm)	Spatially Averaged Grain Size <*D50*> (mm)
FIELD SITE A		6.2
Location 1	1.6	
Location 2	7	
Location 3	10	
FIELD SITE B		7.8
Location 1	10.6	
Location 2	8	
Location 3	4.9	

Bedform heights were measured in outcrop, then mathematically related back to flow depth. Commonly bedforms were incompletely preserved, meaning the paleoflow depths derived from them will be underestimates of the true flow depth. Average bedform height and calculated paleoflow depth is shown for each sampling location in Table 2. Spatially averaged paleoflow depth (<*h*>) for sites A and B were 2.88 and 4.86 meters, respectively.

Values were converted to meters, where necessary, and plugged into Equation 2. Dimensionless depositional slope for sediments at Field Site A was found to be 0.00018, and Field Site B was found to be 0.00015. Error in these values comes from both calculating paleoflow depth and the paleoslope calculations themselves. For paleoflow depth, Allen (1968) presented a plot of flow depth versus bedform heights and a best fit line represented by the relationship shown in Equation 3. An error field was added the plot that included 95% of the data points representing two standard deviations. This was used to establish a ± error for calculated flow depths, shown in Table 4.2. Paleoslope calculations have a factor of two error associated with them. Combined, these errors would give a range of slopes at Field Site A of 0.0001 to 0.00039, and Field Site B of 0.00025 to 0.000083. This range of error is not sufficient to produce the slope values of 0.0010-0.0020 observed bounding the modern Ogallala Formation on the SHP.

In the paleoslope equation, flow depth is inversely proportional to slope. If grain size is not changing and the values for paleoflow depth are truly underestimates, increasing *h* would further decrease paleoslope values. To achieve a slope equaling

that of the modern basal Ogallala Formation surface, paleoflow depth must equal 0.25 meters for Field Site A and 0.35 meters for Field Site B. Given the average bedform heights at Field Site A were greater than 0.25 meters and at Field Site B were considerably greater than 0.35 meters, it would be impossible to produce them in flows of these depths. This further confirms that the modern observed slopes bounding the Ogallala Formation are unreasonably steep and could not possibly represent the depositional slope.

Table 4.2. Paleoflow Depth Data

Location	Average Bedform Height (*b*) (m)	Calculated Flow Depth (*h*) (m)	*h* minus two standard deviations[ɬ]	*h* plus two standard deviations[ɬ]	<*h*> (m)	<*h*> minus two standard deviations	<*h*> plus two standard deviations
FIELD SITE A					**2.88**	1.43	7.10
Location 1	0.29	2.77	1.4	6.9			
Location 2	0.33	3.10	1.5	7.5			
Location 3	0.29	2.77	1.4	6.9			
FIELD SITE B					**4.86**	2.13	11.6
Location 1	0.7	5.82	2.5	14			
Location 2	0.4	3.64	1.7	7.9			
Location 3	0.6	5.11	2.2	13			

CHAPTER V

POST-MIOCENE TILTING OF THE SOUTHERN HIGH PLAINS

Depositional slope values for the Ogallala Formation are nearly an order of magnitude less than the observed modern slopes (Fig. 5.1). These calculations are derived from data at two field sites, one from each member of the Ogallala Formation. Both sites plot near the data trend of modern river slopes for the given distance from

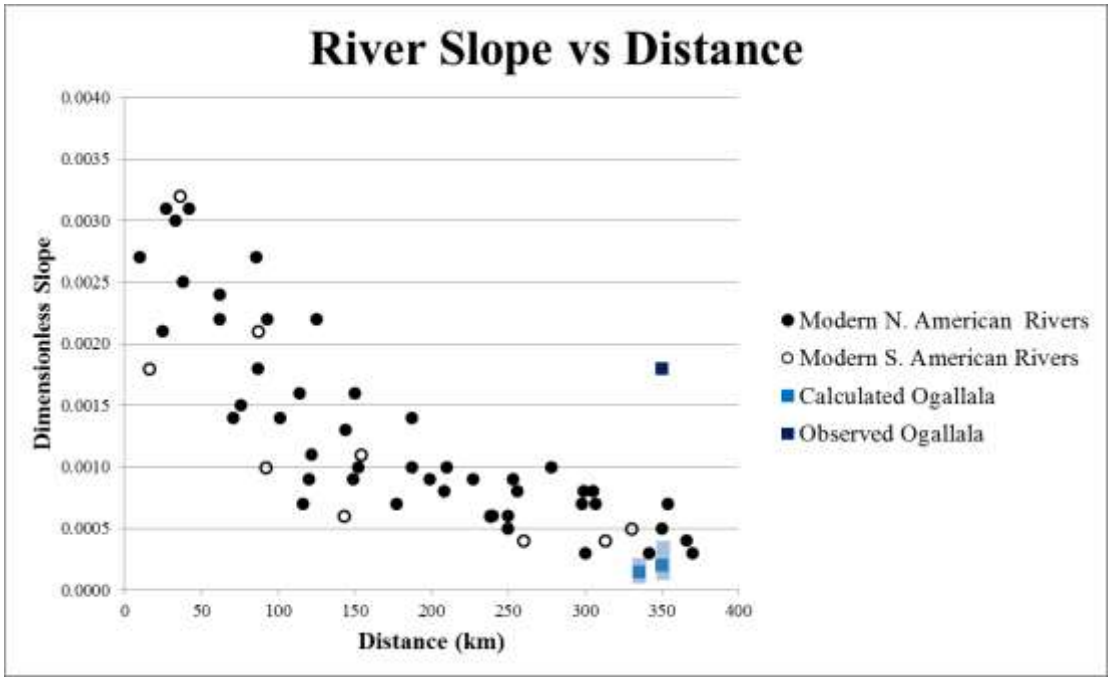

Figure 5.1. River slope plot, with calculated slopes added. Calculated slopes fall near the expected data trend. Error bars appear in light blue and include error from calculating paleoflow depth (Table 4.2) plus a factor of two beyond that to account for error in the paleoslope equation. See Appendix A for data.

the highlands. Discrepancy between depositional slope and slope of modern Ogallala surface implies that the SHP has been tilted post-Ogallala deposition, i.e. late Miocene or later. The surface of the SHP dips to the east, meaning the western margin of the SHP has been preferentially uplifted.

To estimate potential uplift, depositional and modern slopes are projected away over some chosen distance from a fixed point, and the surfaces diverge. The magnitude of terminal divergence is equal to uplift. Data comes from field sites located close to the eastern escarpment, and projecting both depositional and modern slopes westward to the center of the Pecos River Valley from this point equates to ~ 600 meters of relative uplift along the western escarpment (Fig. 5.2).

Possible causes of tilting include: 1) recent tectonic activity, 2) isostatic uplift do to crustal heating, and 3) isostatic uplift due to erosion. To date, no recent tectonic

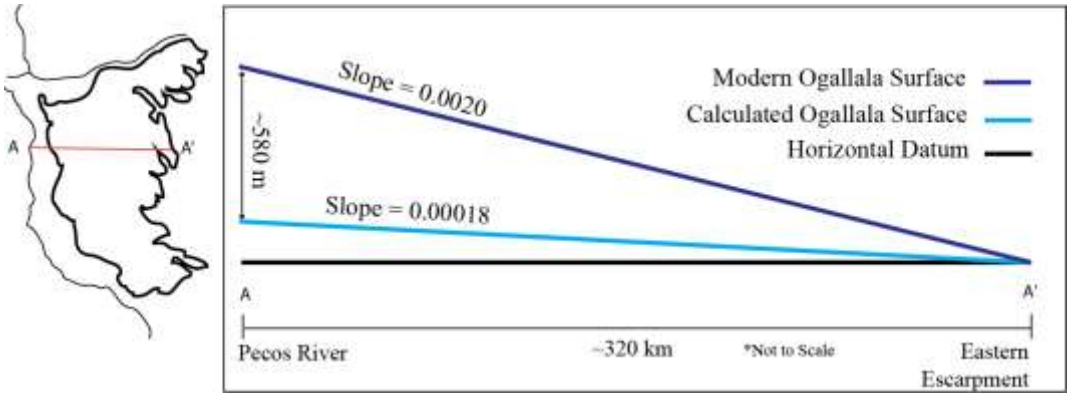

Figure 5.2. Uplift of the SHP along Pecos River relative to the eastern escarpment. Diagram extending the modern and calculated surfaces from the field sites along the eastern escarpment of the SHP to the center of the Pecos River valley. To satisfy the divergence of these surfaces, ~580 meters of uplift is required to the west of the SHP. Not to scale.

activity has been documented along or near the SHP that could account for the necessary magnitude of uplift to reconcile the slopes. Although lack of positive evidence is commonly not a good discriminator, in this case it is hard to argue for a neo-tectonic mechanism without an identified fault. Presence of the Rio Grande Rift to the west of the study area was considered a potential source for mantle heating along the western margin of the SHP. Increased temperature in the asthenosphere would decrease lithospheric mantle density, causing buoyant uplift. Using gravity data, a low-density pocket of mantle has been mapped along the western margin of the SHP (Hoemberg, 2010). In addition to low-density mantle, isostatic response due to river incision could contribute to uplift. The Pecos River has incised ~180 meters in eastern New Mexico since latest Pliocene (Walker, 1978), and the Canadian River has incised ~186 meters along the northern border of the SHP during the same time period (Walker, 1978). While material has also been removed east of the SHP, it was not directly modeled because the increase in slope from depositional to modern times implies that a greater magnitude of uplift has occurred to the west of the SHP. Therefore uplift of the SHP is thought of as a tilting table top, and the differential uplift along the western margin is what needs to be accounted for. A 2-D airy isostasy model was constructed to test isostatic response to both crustal heating and river incision (Fig. 5.3). A fixed datum was set at the base of the lithosphere. Initial conditions were an assumed crustal thickness of 42 kilometers and a mantle thickness of 42 kilometers split into upper and lower components (Hoemberg, 2010) over the average width of the valley in question (85 kilometers for the Pecos River and 90

kilometers for the Canadian River), and a crustal and mantle density of 2.75 g/cm^3 and 3.3 g/cm^3, respectively. Removal of material by the rivers induced an isostatic response, causing the mantle to rise and compensate for the removal of mass. To simplify geometry, the valleys were assumed to be V-shaped and material removed was geometrically converted from a triangle to a rectangle. To test effect of mantle heating, density of the upper 30 kilometers of mantle was lowered to 3.2 g/cm^3, according to the thickness suggested for buoyant mantle west of the SHP by Hoemberg (2010). This resulted in nearly a kilometer of uplift around the Pecos River valley. A mass-balance equation was created to measure the amount of uplift caused by erosion in the Pecos and Canadian river valleys (Fig. 5.3). The initial mass of the lithosphere prior to erosion must equal the mass of the lithosphere after mantle that rises. Estimated rebound using this model was 75 meters from Pecos River incision and 82 meters from Canadian River incision.

While river incision and isostatic adjustment might have played a role, it was minor compared with the magnitude of uplift capable of being produced by lowering density of such a thick zone of mantle. Combining the effect of buoyant mantle and river incision produces ~1000 meters of uplift to the west of the SHP. This value represents absolute uplift from these two sources, while the expected value shown in Figure 5.2 is relative, including contribution from removal along the eastern margin of the SHP. Isostatic response to the east of the plateau would be mirrored by uplift to the west, like the rising of the floor of an elevator. However, the western margin continued to rise, resulting in ~580 meters of differential uplift relative to the east.

Rigidity of the lithosphere surrounding the 2-D area in Figure 5.3 was not modeled and would reduce the effect of isostatic uplift. The 400 meter surplus of uplift generated by mantle buoyancy is likely accounted for by flexure and concurrent uplift along the eastern margin of the SHP. Therefore, uplift driven by mantle buoyancy aided by river incision appears to account for the tilting proposed on the SHP, showing how much of an effect a small change in mantle density can have on the overlying crust.

These findings are similar to those presented by Cather et al. (2012). Ogallala Formation paleoslopes were used to show uplift in western Colorado relative to the east. One kilometer of uplift was estimated along the Front Range of the Rocky Mountains in (Fig. 5.4). River incision seen there only accounted for a few hundred meters of uplift, leaving a ~80% the uplift attributed to mantle processes, possibly related to dynamic processes within the Jemez Lineament.

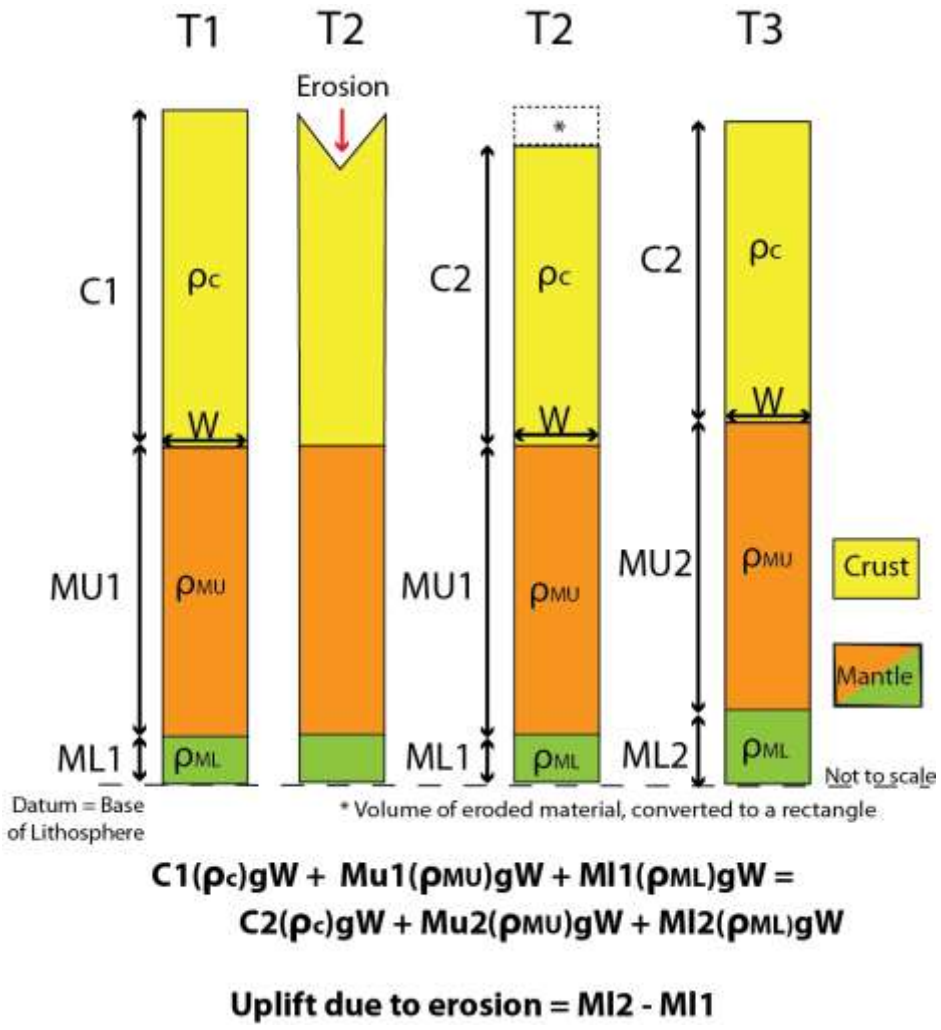

Figure 5.3. 2D Airy Isostasy model. T1: Area in question at the end of Ogallala Formation deposition (late Miocene-early Pliocene), before any crust was removed. T2: Formation of the river valley (late Pliocene-Present). The valley is assumed to be V-shaped. The column is redrawn so that area of removed strata is represented as a rectangle to simplify geometry and calculations. T3: Isostatic response due to removal of crust. Mantle rises to compensate for erosion. ML2 minus ML1 is equal to the amount of uplift. W = average width of the river valley, C1 = crustal thickness before erosion, ρ_c = crustal density = 2.75 g/cm^3, C2 = crustal thickness post-erosion, MU1 = MU2 = upper mantle thickness, ρ_{MU} = upper mantle density = 3.3 g/cm^3, ML1 = lower lithospheric mantle thickness, ML2 = thickness of lower mantle after rebound, ρ_{ML} = mantle density 3.3 g/cm^3. Uplift due to incision is the difference between ML2 and ML1. To test effect of mantle heating, upper mantle density was lowered to 3.2 g/cm^3.

Figure 5.4. Model of uplift along Front Range in Colorado using Ogallala Formation depositional slopes. Diagram from a study showing how modern and depositional slopes of the Ogallala Formation have been used to argue for tilting in the midcontinent of the U.S.. This study estimated uplift value of ~ 1 kilometer along the Front Range of the Rocky Mountains. From Cather et al. 2012.

CHAPTER VI

CONCLUSIONS

Paleoslope reconstructions of the Ogallala Formation on the SHP are an order of magnitude less than the modern observed slopes, implying tilting of the SHP since the formation was deposited. The airy isostatic model presented in this study indicates that ~one kilometer of uplift occurred along the western margin of the SHP through mantle buoyancy and isostatic rebound following river incision. Approximately 580 meters of relative uplift were expected around the Pecos River based on the difference in depositional and modern observed slopes for the Ogallala Formation. Given the rigid nature of the crust outside of the area modeled, coupled with the concurrent uplift along the eastern margin of the SHP, this magnitude of relative uplift can be explained by mantle buoyancy plus a small component of isostatic rebound due to river incision in the west and north. These findings support similar work conducted on the Ogallala Formation to the north of this study area in Colorado, showing that small changes in mantle density can have a significant effect on surface topography.

REFERENCES CITED

Allen, J. R. L., 1968, Current Ripples: Their relation to patterns of water and sediment motion: North-Holland Publishing Co., Amsterdam, 433 p.

Barnes, V. E., Eifler, G.K., Reeves, C.C., Kottlowski, F.E., Quackenbush, W.M., Grant, W.D., and Hughes, C.D., 1977, Geologic atlas of Texas, Clovis sheet: scale 1:250,000, Bureau of Economic Geology, University of Texas at Austin.

Blakey, R., 2011, Global paleogeography, NAU Geology. Northern Arizona University, Flagstaff, USA.

Bretz, J. H., and Horberg, L., 1949, The Ogallala formation west of the Llano Estacado: The Journal of Geology, v. 57, p. 477-490.

Bridge, J., and Demicco, R., 2008, Earth surface processes, landforms and sediment deposits: Cambridge University Press, 815 p.

Cather, S. M., Chapin, C. E., and Kelley, S. A., 2012, Diachronous episodes of Cenozoic erosion in southwestern North America and their relationship to surface uplift, paleoclimate, paleodrainage, and paleoaltimetry: Geosphere, v. 8, no. 6, p. 1177-1206.

Cope, E. D., 1893, A preliminary report on the vertebrate paleontology of the Llano Estacado: Austin, TX, BC Jones, state printers, Fourth Annual Report, 152 p.

Cox, E. R., 1967, Geology and hydrology between Lake McMillan and Carlsbad Springs, Eddy County, New Mexico: USGS, Water Supply Paper no. 1828, 48 p.

Cronin, J. G., 1969, Ground water in the Ogallala formation in the Southern High Plains of Texas and New Mexico: U.S. Geological Survey Hydrologic Investigations HA-330, 9 p.

Dickinson, W. R., and Snyder, W. S., 1978, Plate tectonics of the Laramide orogeny: Geological Society of America Memoirs, v. 151, p. 355-366.

Eifler, G., Frye, J., Leonard, A., Hentz, T., and Barnes, V., 1967, Geologic Atlas of Texas, Lubbock Sheet: scale 1:250,000, Bureau of Economic Geology, University of Texas at Austin.

Frye, J. C., and Leonard, A. B., 1964, Relation of Ogallala Formation to the Southern High Plains in Texas: Austin, TX, Bureau of Economic Geology, University of Texas, Report of Investigations no. 51, 25 p.

Gustavson, T. C., and Winkler, D. A., 1988, Depositional facies of the Miocene-Pliocene Ogallala Formation, northwestern Texas and eastern New Mexico: Geology, v. 16, no. 3, p. 203-206.

Hawley, J., 1993, The Ogallala and Gatuña Formations in the southeastern New Mexico region, a progress report: Carlsbad region, New Mexico and west Texas: New Mexico Geological Society, Guidebook, v. 44, p. 261-269.

Heller, P. L., Dueker, K., and McMillan, M. E., 2003, Post-Paleozoic alluvial gravel transport as evidence of continental tilting in the U.S. Cordillera: GSA Bulletin, v. 115, no. 9, p. 1122-1132.

Hoemberg, Jeffrey, 2010, Characterization of the Southern High Plains by seismic, gravity, and topographic analysis: Texas Tech University, Lubbock, Texas, 149 p.

Holliday, V. T., 1989, The Blackwater Draw Formation (Quaternary): A 1-4-plus-my record of eolian sedimentation and soil formation on the Southern High Plains: Geological Society of America Bulletin, v. 101, no. 12, p. 1598-1607.

-, 1990, Soils and landscape evolution of eolian plains: the Southern High Plains of Texas and New Mexico: Geomorphology, v. 3, no. 3, p. 489-515.

Izett, G., and Obradovich, J., 2001, ^ 4^ 0Ar/^ 3^ 9Ar Ages of Miocene Tuffs in Basin-Fill Deposits (Santa Fe Group, New Mexico, and Troublesome Formation, Colorado) of the Rio Grande Rift System: Mountain Geologist, v. 38, no. 2, p. 77-85.

Johnson, W. D., 1901, The High Plains and their utilization: 21st Annual Report, U.S. Geological Survey, part 4, p. 609-741.

Leonard, E. M., 2002, Geomorphic and tectonic forcing of late Cenozoic warping of the Colorado piedmont: Geology, v. 30, no. 7, p. 595-598.

Lucas, S. G., and Anderson, O. J., 1993, Stratigraphy of the Permian-Triassic boundary in southeastern New Mexico and west Texas, in *Proceedings Geology of the Carlsbad Region, New Mexico and West Texas*: 44th NMGS Fall Field Conference Guidebook, New Mexico Geological Society, Socorro, NM, p. 219-230.

Machette, M. N., 1985, Calcic soils of the southwestern United States: Geological Society of America Special Papers, 203, p. 1-22.

McMillan, M. E., Angevine, C. L., and Heller, P. L., 2002, Postdepositional tilt of the Miocene-Pliocene Ogallala Group on the western Great Plains: Evidence of late Cenozoic uplift of the Rocky Mountains: Geology, v. 30, no. 1, p. 63-66.

Paola, C., and Mohrig, D., 1996, Paleohydraulics revisited: paleoslope estimation in coarse-grained braided rivers: Basin Research, v. 8, p. 243-254.

Parker, G., Klingeman, P. C., and McLean, D. G., 1982, Bedload and size distribution in paved gravel-bed streams: Journal of the Hydraulics Division, v. 108, no. 4, p. 544-571.

Reeves Jr, C., 1976, Quaternary stratigraphy and geologic history of southern High Plains, Texas and New Mexico, in *Quaternary Stratigraphy of North America*: Dowden, Hutchinson, & Ross Stroudsburg, PA, p. 213-234.

- Jr, C., 1970, Origin, classification, and geologic history of caliche on the southern High Plains, Texas and eastern New Mexico: The Journal of Geology, v. 78, no. 3, p. 352-362.

Schultz, Gerald, 1977, The Ogallala Formation and its vertebrate faunas in the Texas and Oklahoma panhandles, in *Proceedings Guidebook; field conference on late Cenozoic biostratigraphy of the Texas Panhandle and adjacent Oklahoma*: West Texas State University, Canyon, TX, Special Publication 1, p. 5-104.

-, 1990, Clarendonian and Hemphillian vertebrate faunas from the Ogallala Formation (late Miocene–early Pliocene) of the Texas Panhandle and adjacent Oklahoma: in *Geologic framework and regional hydrology: Upper Cenozoic Blackwater Draw and Ogallala Formations, Great Plains*: p. 56-96.

Seni, S. J., 1980, Sand-Body Geometry and Depositional Systems, Ogallala Formation, Texas: Austin, TX, Bureau of Economic Geology, Report of Investigations No.105, 39 p.

Tedford, R., Skinner, M., Fields, R., Rensberger, J., Whistler, D., Galusha, T., Taylor, B., Macdonald, J., and Webb, S., 1987, Faunal succession and biochronology of the Arikareean through Hemphillian interval (late Oligocene through earliest Pliocene epochs): in *North America, Cenozoic mammals of North America: geochronology and biostratigraphy*: p. 153-210.

Tedford, R. H., Albright III, L. B., Barnosky, A. D., Ferrusquia-Villafranca, I., Hunt Jr, R. M., Storer, J. E., Swisher III, C. C., Voorhies, M. R., Webb, S. D., and Whistler, D. P., 2004, Mammalian biochronology of the Arikareean through Hemphillian interval (late Oligocene through early Pliocene epochs) in *Late Cretaceous and Cenozoic mammals of North America: biostratigraphy and geochronology*: p. 169-231.

Walker, J. R., 1978, Geomorphic evolution of the Southern High Plains, Baylor University, Department of Geology, Baylor Geological Studies Bulletin No. 35, p 6-25.

Winkler, D. A., 1987, Vertebrate-bearing eolian unit from the Ogallala Group (Miocene) in northwestern Texas: Geology, v. 15, no. 8, p. 705-708.

-, D. A., 1990, Sedimentary Facies and Biochronology of the Upper Tertiary Ogallala Group, Blanco and Yellow House Canyons, Texas Panhandle in *Geologic framework and regional hydrology: Upper Cenozic Blackwater Draw and Ogallala Formations, Great Plains*: p. 39-55.

Wisniewski, P. A., and Pazzaglia, F. J., 2002, Epeirogenic controls on Canadian River incision and landscape evolution, Great Plains of northeastern New Mexico: The Journal of Geology, v. 110, no. 4, p. 437-456.

Woodburne, 2004, Principles and Procedures: in *Late Cretaceous and Cenozoic Mammals of North America: Biostratigraphy and Geochronology*: Columbia University Press, p. 1-20.

APPENDIX A

River Slope Data

River Slope Database

River	Distance Downstream (km)	Dimensionless Slope	Latitude	Longitude
Arkansas	71	0.0014	38.475442	-105.8867
Arkansas	149	0.0009	38.400501	-105.11853
Big Horn	240	0.0006	46.163092	-107.46673
Big Horn	300	0.0003	46.283341	-106.84043
Bow	33	0.003	51.214392	-114.62018
Bow	114	0.0016	50.811905	-113.74568
Bow	187	0.0010	50.775674	-112.78884
Bow	250	0.0006	50.524813	-112.36303
Bow	298	0.0007	50.212546	-111.98458
Bow	370	0.0003	49.904235	-111.58809
N Fork Platte	62	0.0022	41.213613	-104.82274
N Fork Platte	5	0.0097	42.228646	-104.65412
N Fork Platte	250	0.0005	41.232653	-101.76687
N Fork Platte	101	0.0014	42.20742	-104.56214
N Fork Platte	120	0.0009	41.727888	-103.24098
N Fork Platte	208	0.0008	41.3554414	-102.28021
North Saskatchewan	187	0.0014	53.056164	-115.12621
North Saskatchewan	253	0.0009	53.357611	-114.39616
North Saskatchewan	307	0.0007	53.357697	-113.76491
North Saskatchewan	366	0.0004	53.628921	-113.27962
Powder	87	0.0018	43.835966	-106.24721
Powder	122	0.0011	44.242172	-106.15609
Powder	177	0.0007	44.731508	-106.11084
Powder	227	0.0009	45.117183	-105.84082

Powder	278	0.0010	45.431928	-105.39272
Powder	305	0.0008	45.661640	-105.24791
Powder	354	0.0007	46.025949	-105.05683
Sun	10	0.0027	47.647604	-112.5437
Sun	27	0.0031	47.546558	-112373362
Sun	62	0.0024	47.511793	-112.00021
Sun	116	0.0007	47.502012	-111.35527
Tongue	25	0.0021	44.905722	-107.07829
Tongue	76	0.0015	45.228033	-106.67027
Tongue	152	0.001	45.832882	-106.22624
Tongue	199	0.0009	46.118933	-105.83371
Upper Cimarron	25	0.0060	36.674756	-103.03273
Upper Cimarron	42	0.0031	36.596594	-102.8447
Wind	24	0.0064	43.452471	-109.4755
Wind	86	0.0027	43.195252	-108.83074
Wind	125	0.0022	42.981985	-108.4651
Wind	144	0.0013	43.121169	-108.2451
Yellowstone	38	0.0025	45.565906	-110.61778
Yellowstone	93	0.0022	45.771115	-110.12154
Yellowstone	150	0.0016	45.682005	-109.42918
Yellowstone	210	0.0010	45.671227	-108.68692
Yellowstone	299	0.0008	46.08229	-107.68501
Yellowstone	350	0.0005	46.313049	-107.18101
Yellowstone	256	0.0008	46.513646	-105.72903
Yellowstone	342	0.0003	46.902889	-104.9392
Rio Grande O Guapay	92	0.0010	-18.804349	-63.289003
Rio Grande O Guapay	154	0.0011	-18.804349	-62.887207
Rio Grande O Guapay	16	0.0018	-19.044071	-63.724488
Rio Grande O Guapay	260	0.0004	-17.547402	-62.790177
Rio Grande O Guapay	330	0.0005	-17.047334	-62.990889

Pilcomayo	36	0.0032	-21.140201	-63.95674
Pilcomayo	87	0.0021	-21.264985	-63.501208
Pilcomayo	143	0.0006	-21.507766	-63.081795
Pilcomayo	238	0.0006	-22.25666	-62.656424
Pilcomayo	313	0.0004	-22.634904	-62.244400

APPENDIX B

Sieve Set up and Grain Size Distributions

Sieve Setup

Sieve No.	mm	Φ
-	9.5	-3.25
4	4.75	-2.25
5	4	-2
8	2.36	-1.25
10	2	-1
16	1.18	-0.25
18	1	0
20	0.85	0.25
30	0.6	0.75
35	0.5	1
40	0.425	1.25
50	0.3	1.75
60	0.25	2
80	0.18	2.5
100	0.15	2.75
120	0.12	3
140	0.106	3.25
170	0.088	3.5
230	0.63	4
Pan	<0.63	-

Grain Size Distributions

Field Site A, Sampling Location 1

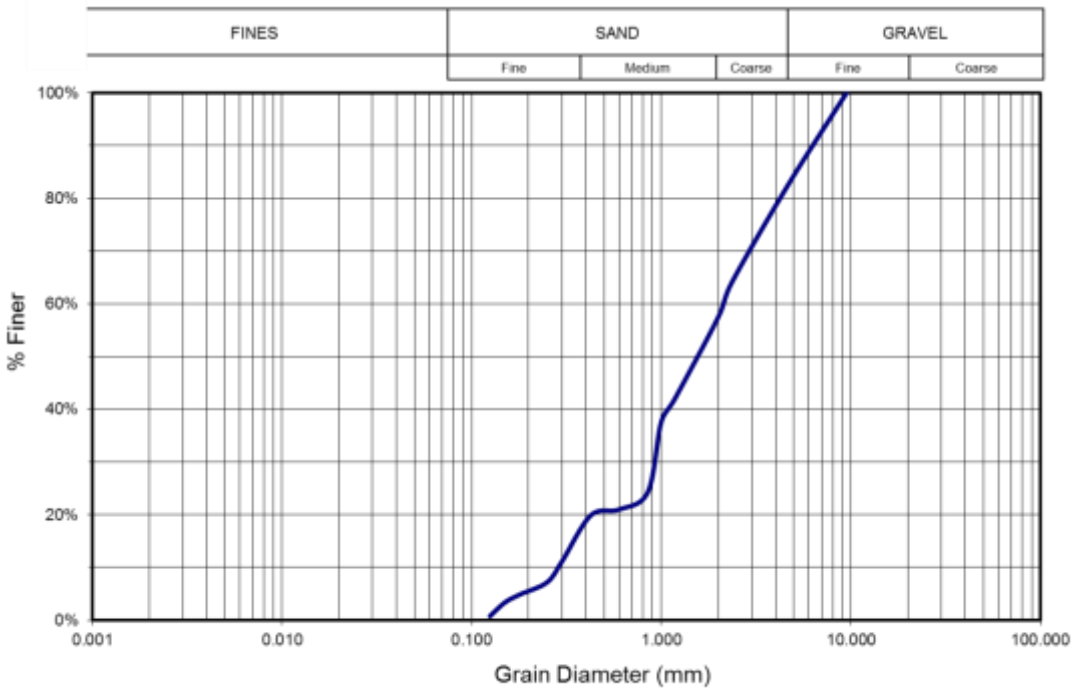

Field Site A, Sampling Location 2

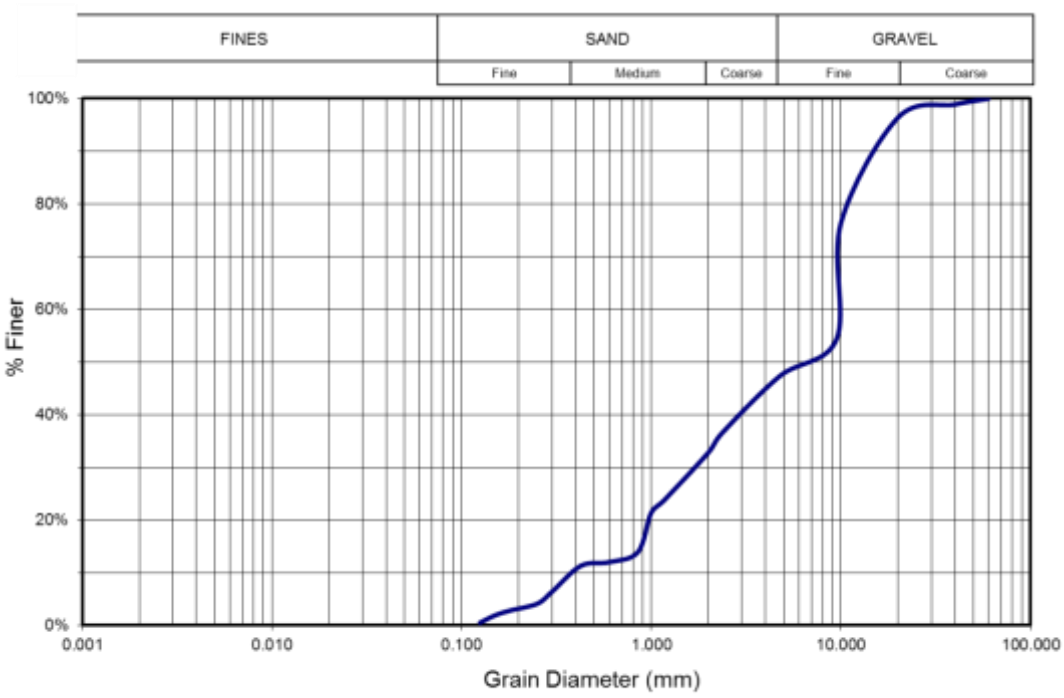

Field Site A, Sampling Location 3

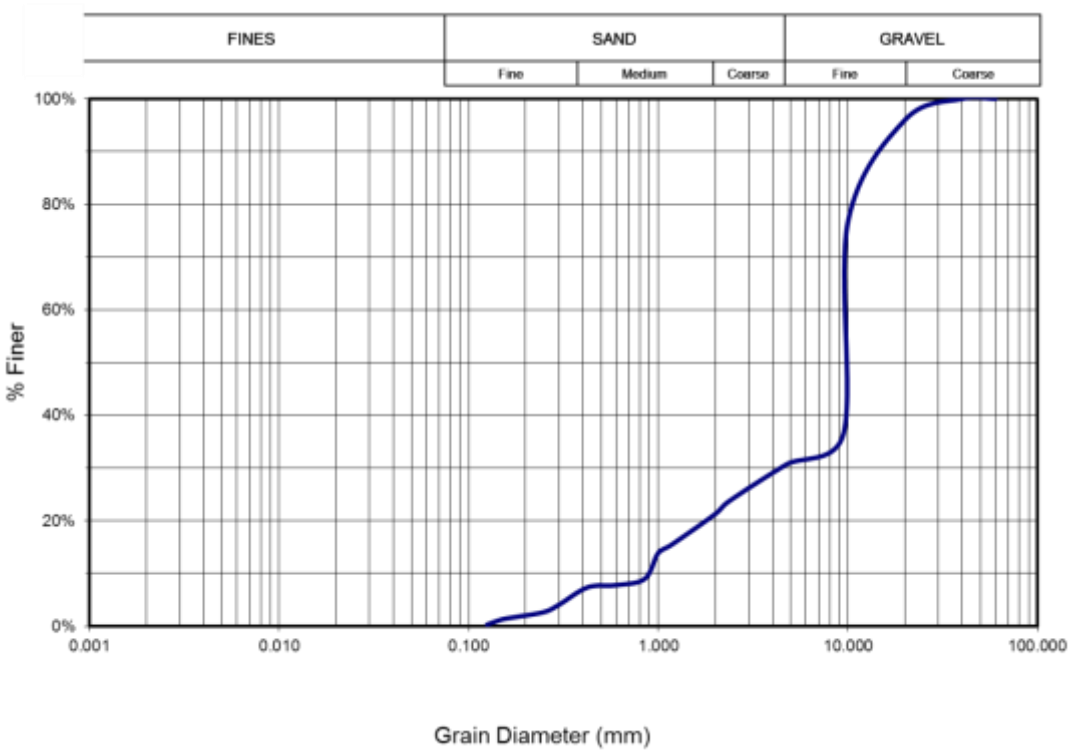

Field Site B, Sampling Location 1

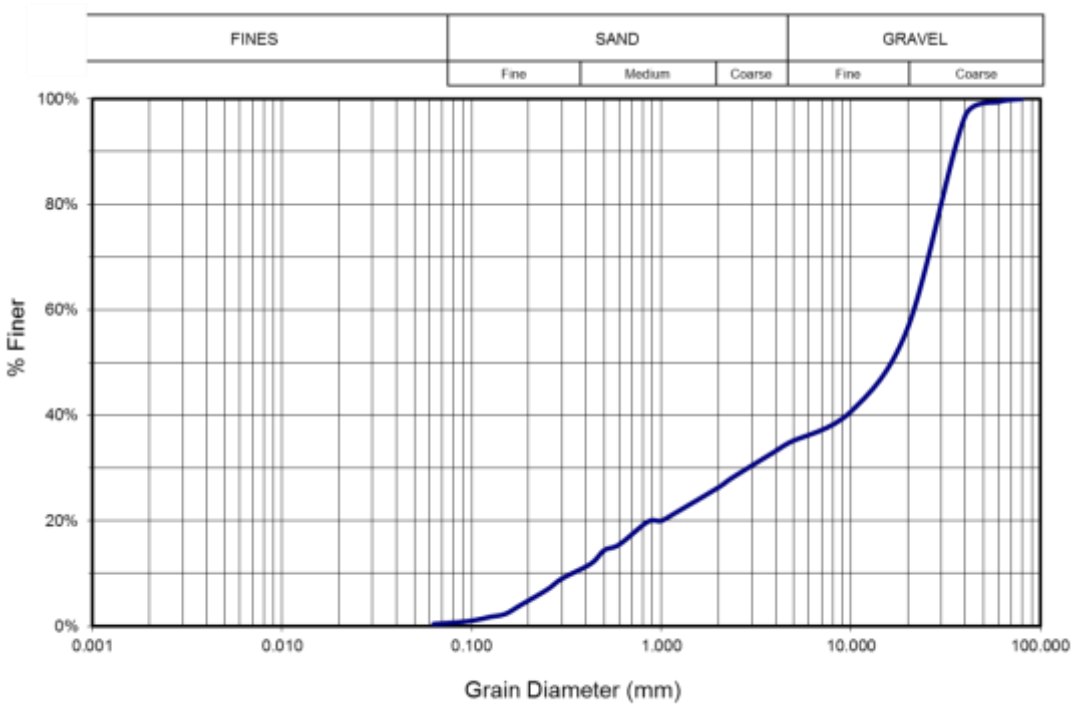

Field Site B, Sampling Location 1

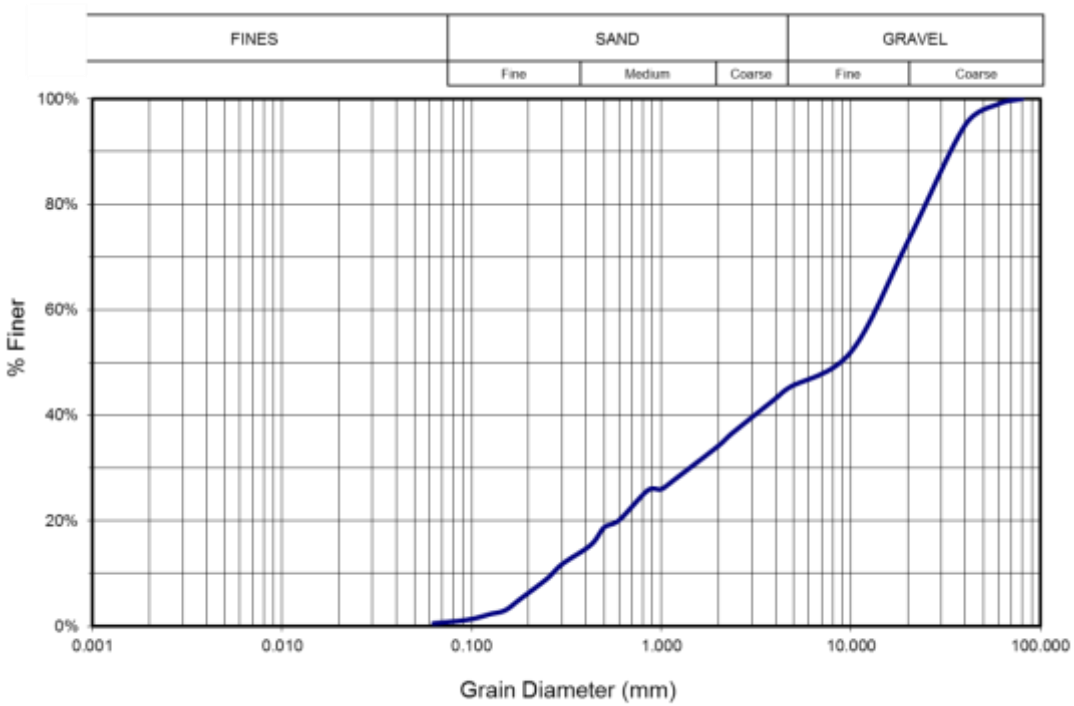

Field Site B, Sampling Location 1